Observation of Peierls transition in nanowires (diameter ∼ 130 nm) of the charge transfer molecule TTF–TCNQ synthesized by electric-field-directed growth

T Phanindra Sai[1] **and A K Raychaudhuri**[1,2]

[1] Department of Physics, Indian Institute of Science, Bangalore 560012, India
[2] Unit for Nanoscience, S N Bose National Centre for Basic Sciences, Kolkata 700098, India

E-mail: phanindra@physics.iisc.ernet.in

Abstract

We report the growth of nanowires of the charge transfer complex tetrathiafulvalene–tetracyanoquinodimethane (TTF–TCNQ) with diameters as low as 130 nm and show that such nanowires can show Peierls transitions at low temperatures. The wires of sub-micron length were grown between two prefabricated electrodes (with sub-micron gap) by vapor phase growth from a single source by applying an electric field between the electrodes during the growth process. The nanowires so grown show a charge transfer ratio ∼0.57, which is close to that seen in bulk crystals. Below the transition the transport is strongly nonlinear and can be interpreted as originating from de-pinning of CDW that forms at the Peierls transition.

1. Introduction

There has been considerable interest in the synthesis, design and characterization of organic charge transfer (CT) salts, a class of molecules in which metallic conductivity and even superconductivity has been observed [1]. Conducting organic micro-and nanowires are useful for constructing efficient all-organic electronic devices. Charge transfer molecules have, for a long time, been considered as promising candidates for organic molecular conductors. Until recently studies on charge transfer complexes have been concentrated almost exclusively on single crystals. Most well-studied charge transfer molecules are complexes of TTF–TCNQ in single-crystalline form or thin film form [2–7]. TTF–TCNQ is a typical one-dimensional charge transfer compound with monoclinic crystal structure having lattice constants $a = 1.2298$ nm, $b = 0.3819$ nm, $c = 1.8468$ nm and $\beta = 104.46°$ [8]. The structure consists of TTF and TCNQ stacks. TTF is a strong electron donor, while TCNQ is an electron acceptor with a charge transfer ratio ∼0.59. The molecules are tilted with respect to the chain axes. Along the stacks the π-orbitals overlap, leading to one-dimensional conductivity. Single crystals of charge transfer (CT) complexes like that of TTF–TCNQ show a Peierls transition at temperatures in the vicinity of 38–55 K. Such a transition leads to charge density wave (CDW) formation. Below the Peierls transition the charge transport takes place through the motion of CDW. TTF–TCNQ belongs to quasi-one-dimensional conductors having high electronic conduction along the b axis. Single crystals exhibit a metal-like conductivity at high temperature, which is suppressed by two successive Peierls transitions on the TCNQ and TTF stacks at 54 K and 38 K, respectively. We show here that nanowires of the molecular complex TTF–TCNQ (sometimes referred to as 'molecular wires') can be synthesized between two prefabricated electrodes using an applied field and also establish that such wires can show a Peierls transition at a similar temperature to the bulk single-crystalline samples.

The single crystals, even though providing clean systems for investigating the underlying physical processes, are fragile and are difficult to process. This limits the prospects for

their practical applications. Recent studies have shown that TTF–TCNQ charge transfer molecular electrodes can be used to replace the regular metal source–drain electrodes for organic thin film transistors with almost the same contact resistance as the metal electrodes [9, 10]. Organic nanochannel FET has been recently fabricated using TTF–TCNQ nanowires [11]. These recent developments have renewed the interest in TTF–TCNQ and in particular attempts have been made to obtain them in the nanometer range of sizes as molecular wires. We are interested in growing nanowires of CT complexes (molecular wires) in a controlled way and studying the electrical characteristics of single molecular wires. Electrical measurements on single or few molecular wires can be done if the wires can be made to grow between prefabricated metal electrodes. In this paper we report electric-field-assisted growth of molecular wires (with diameter ∼130 nm) between prefabricated electrodes and establish through electrical resistance measurements that they can be of good enough quality so that the Peierls transition can be observed. Establishing that such fundamental phenomena like the Peierls transition can be observed in molecular wires as in bulk single crystals is important because this validates the essential one-dimensional (electronic) character of the molecular wires. Though there are reports of growth of molecular wires (albeit of larger length (∼20 μm) and diameter (∼500 nm) [11] there are no measurements done on such wires down to low enough temperatures so that the Peierls transition can be observed. The purpose of this brief report is to show that, in small molecular wires (of sub-micron length and such small diameter), one can indeed observe the transition in the designated temperature range and there is strong evidence that the nonlinear transport seen in these nanowires can arise from de-pinning of CDW that form at the transition [12].

There are different techniques of growing molecular wires. In the Langmuir–Blodgett technique, a long amphiphilic chain is attached to either donor or acceptor molecules and transferred onto a substrate [13]. TTF–TCNQ nanowires of different morphologies were grown by a two-phase chemical solution method [14]. TTF–TCNQ nanowires were also grown on stainless steel conversion coating (SSCC) substrates using the combined technique of chemical vapor deposition (CVD) and further dipping of the substrates in TTF and TCNQ solutions [15]. There are successful reports of growing molecular wires by thermal evaporation method where they are formed between prefabricated electrodes where the alignments have been done by applying an electric field (both DC and AC) [16, 17]. In this paper we report electric-field-assisted growth of a few molecular wires of TTF–TCNQ between prefabricated electrodes. The advantage of this technique is that the prefabricated electrodes also act as electrodes attached to one, or at most a few, wires and thus allow direct electrical measurements. Also the measurements can be done on one or a few molecular wires, as opposed to films where the measurements are done on ensembles of such molecular wires where the number of wires on which measurements have been made cannot be ascertained. The wires so made have their lengths determined by the electrode separation. The previously reported lengths (as determined by the electrode separation) were ∼20 μm and diameter ∼500 nm where the electrodes were fabricated by shadow masks [11]. In this paper we report the synthesis of nanowires across preformed electrodes where the electrode gap has been reduced to the sub-micron region (∼600 nm) and the wires so grown have a diameter of ∼130 nm each. The e-beam lithography technique was used to fabricate the electrodes in order to get more control on positioning of the wires. The size of the molecular wires grown here are much smaller than those grown previously. The small gap is needed to synthesize molecular wires of much smaller diameters.

2. Experimental details

The molecular wires were prepared by the thermal evaporation method on SiO_2 substrates, on which electrodes were prefabricated by using e-beam lithography and the lift-off process. The e-beam lithography was done using polymethylmethacrylate (PMMA) as a resist and the patterns were drawn on the resist-coated substrates by a scanning electron microscope (FEI Quanta 200) with an e-beam lithography attachment and writing software (Nabity). The exposed resists were developed and the developed patterns were metallized with 5 nm chromium and 30 nm gold in a vacuum chamber at a pressure of 2.5×10^{-6} mbar. The PMMA was lifted off in acetone and the lithographic pattern remained on the substrate. These substrates were then placed in another vacuum chamber for evaporation of the charge transfer molecules.

The charge transfer molecules were evaporated from a ceramic boat placed on a heater attached to a temperature controller. The evaporation source was powdered TTF–TCNQ (from Sigma-Aldrich). During evaporation the substrate was maintained at 300 K and the crucible containing TTF–TCNQ was maintained at a temperature of 393 K. A DC bias was applied across the bare metal electrodes on the substrate during the evaporation process. Depending upon the gap between the electrodes, voltages between 0.5 and 5 V were applied. For the sample studied in this work the gap between the electrodes was 600 nm, the width of the electrodes was 1.3 μm and a bias of 0.5 V was applied across the electrodes. The current across the electrodes is simultaneously monitored using a picoammeter, so as to stop evaporation by closing the mechanical shutter as soon as the molecular wire makes contact across the electrodes. Details of the evaporation chamber and other details of sample fabrication are given elsewhere [18].

The TTF–TCNQ molecular wires were also characterized by x-ray diffraction (XRD), Fourier-transform infrared (FTIR) spectroscopy and transmission electron microscopy (TEM). For these characterizations TTF–TCNQ was thermally evaporated in the same vacuum chamber on an SiO_2 substrate for XRD, on a KBr substrate for FTIR and on a TEM grid for TEM studies using the same protocol and evaporation parameters such as temperature and time of growth. This ensures that the material so grown as the film is chemically similar to the molecular wires.

For electrical measurements (resistance and I–V characteristics) the same two leads that were used for applying bias during growth have been used as contacts to make two-probe

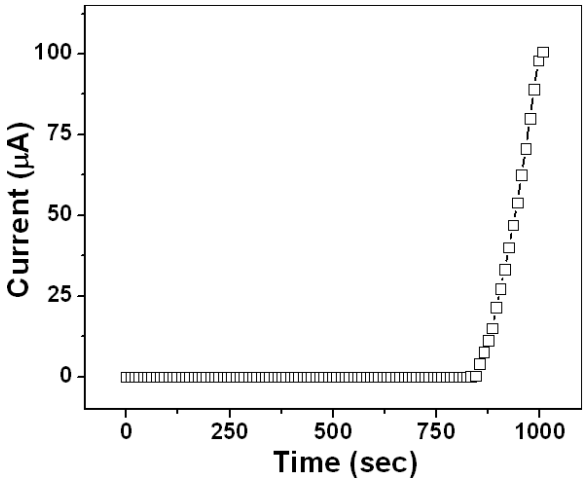

Figure 1. Typical current observed during growth between the prefabricated electrodes for an applied bias of 0.5 V.

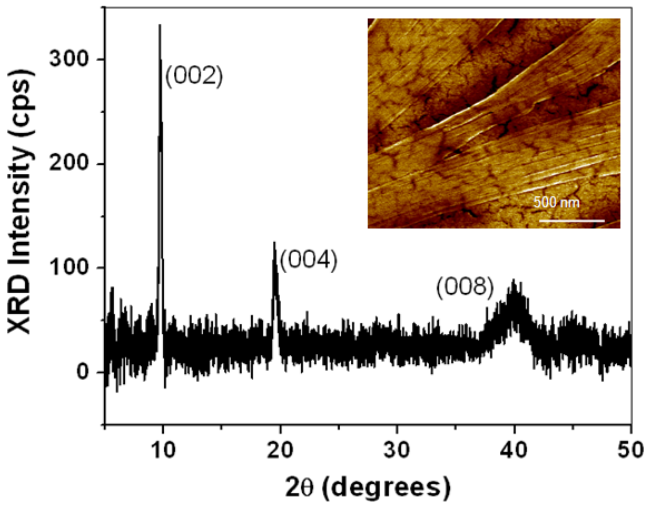

Figure 2. X-ray diffraction pattern from the TTF–TCNQ wires. The inset shows the SEM image of a film of the nanowires.

measurements. The contacts to the leads are rugged and the resistance values are reproducible on many thermal cycles down to low temperatures. The temperature-dependent resistance of the molecular wires grown by this method was measured by passing a constant current of 10 nA from a constant current source and measuring the voltage drop across the sample by high input impedance electrometer, which has an input impedance of 10^{14} Ω. This allows us to measure the resistance of the wires up to 10^{10} Ω, which is the range of resistance at low temperatures. The resistance measurements were carried out in the temperature range 5–300 K in a bath-type cryostat. The current–voltage curves were taken by ramping the voltage across the sample by a voltage source and measuring the current through the sample by an electrometer.

3. Results

In figure 1 the variation of current measured during the evaporation between the two electrodes across which the voltage is applied has been shown as a function of growth time. A DC bias of 0.5 V was applied across the electrodes during deposition and the current starts rising typically after some time (depending on the flux for evaporation) and when it reaches around 100 μA, the deposition was stopped by using the mechanical shutter. By this process we could control the number of grown wires typically from 1 to 5. In figure 2 the XRD pattern obtained for the TTF–TCNQ film grown on the SiO_2 substrate for the same duration as the main sample is shown. The SEM image of the film (as shown in the inset of figure 2) contains an assembly of molecular wires of similar or somewhat larger dimensions. TTF–TCNQ grows in a $P2_{1c}$ space group with a monoclinic crystal structure. From the XRD pattern in figure 2 it can be seen that only (0, 0, l) reflections for even values of l occur, which is usually the case for thermally sublimated TTF–TCNQ thin films [7, 15], whereas TTF–TCNQ nanowires grown by the chemical solution method have shown all the known reflections of the $P2_{1c}$ space group, as can be seen in [14].

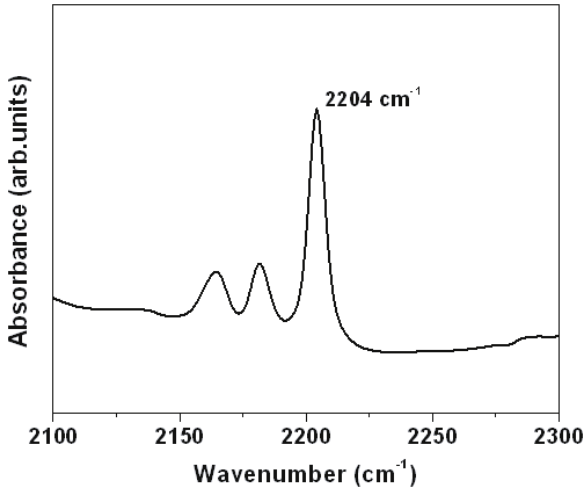

Figure 3. The FTIR data taken on an ensemble of TTF–TCNQ nanowires grown on KBr.

In figure 3 the FTIR spectra of the wires grown on KBr substrate has been shown. The exact frequency of vibration modes depends on whether the molecule is charged or not. The shift in the frequency in the vibrational spectra for neutral molecules to that of ionized molecules can be used to determine the degree of charge transfer. The C≡N stretching mode of TCNQ is a mode which gives a large ionization shift and hence is generally used in the determination of charge transfer in TCNQ-based compounds. From the obtained FTIR data, the C≡N stretching mode was observed at 2204 cm^{-1} whereas for neutral TCNQ this mode should be observed at 2223 cm^{-1}. Chappell [12] has studied many compounds of TCNQ and has given a plot of frequency and degree of charge transfer, which was used as a reference plot to obtain the degree of charge transfer, which in our case is ≈0.57. The estimated charge transfer $Z \approx 0.57$ is very close to $Z = 0.59$ found in single crystals of TTF–TCNQ [15, 19]. The other two small peaks observed in the FTIR spectrum correspond to A_g and B_u

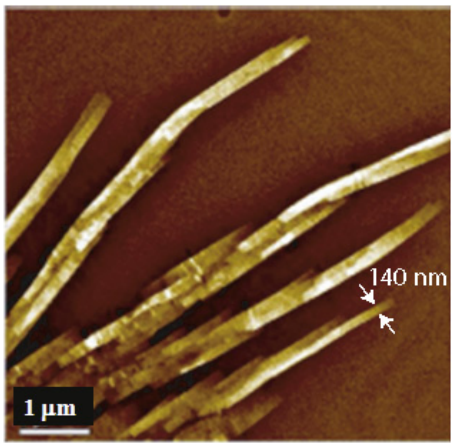

Figure 4. TEM images of the grown nanowires.

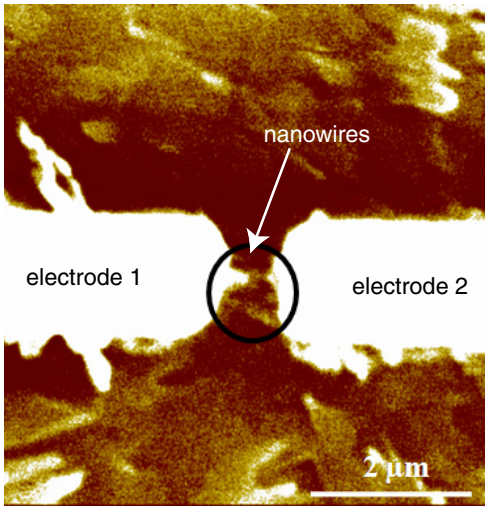

Figure 5. SEM image of the wires (in the marked area), grown between the prefabricated electrodes.

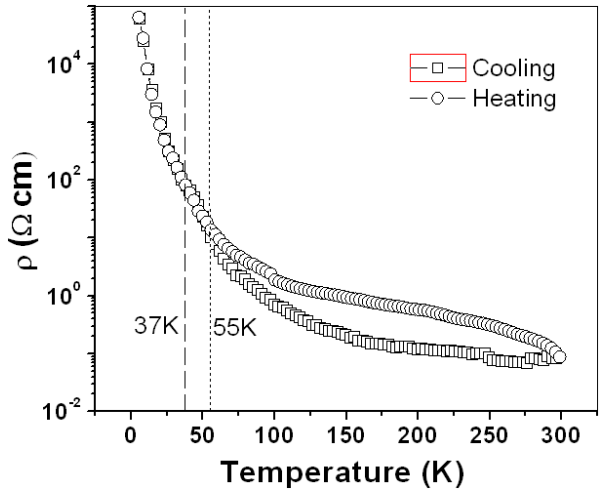

Figure 6. Resistivity of the nanowires as a function of temperature. The hysteresis between the heating and cooling curves can also be seen during thermal cycling.

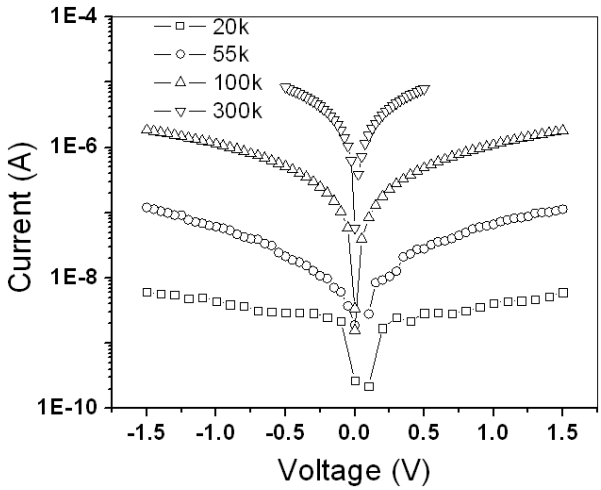

Figure 7. Typical I–V curves taken on the nanowires at different temperatures.

modes of $TCNQ^{-1}$, which were also observed for many TCNQ salts.

In figure 4 we show the TEM image of wires grown directly on a TEM grid, where the wires have diameters of around 140 nm. Often the wires grow in clusters of 3–4 wires and the diameter of the wires may appear larger. In figure 5 we show the SEM images of the sample as grown between the electrodes. The diameter of each molecular wire was measured to be approximately 130–150 nm and it can be seen from the particular image that there are five such wires (marked by arrows). Growth of molecular wires has also occurred away from the electrodes, but since they do not bridge the gap between the electrodes they do not make any contribution to the electrical conductivity. The samples used for TEM imaging were grown directly on TEM grids without electric fields for the same length of time as the sample shown in figure 5. This gives rise to random growth of wires but of similar diameters. We find that, when the growth conditions are kept constant, the wires grown by this method have diameters that are reproducible.

The resistivity of the molecular wires as a function of temperature is shown in figure 6, where they show semiconductor-like behavior. There is sharp raise in resistivity below 55 K, which is around the same temperature below which the Peierls transition occurs on TCNQ stacks. The molecular wires grown by thermal evaporation do not show the metallic behavior, as the stoichiometry of the wires does not remain 1:1 due to different vapor pressures of TTF and TCNQ molecules and these wires formed are generally TCNQ-rich [2, 16, 17]. It is also observed in figure 6 that there is hysteresis between the cooling and heating curves above the Peierls transition temperature, which persists all the way to room temperature. Hysteresis has been observed in resistivity as a function of temperature in TTF–TCNQ around the Peierls transition temperatures of 38 and 52 K but it does not persist to room temperature [20].

An important characteristic of the electrical transport in these systems is nonlinear transport that becomes very prominent below the Peierls transition. Figure 7 shows the

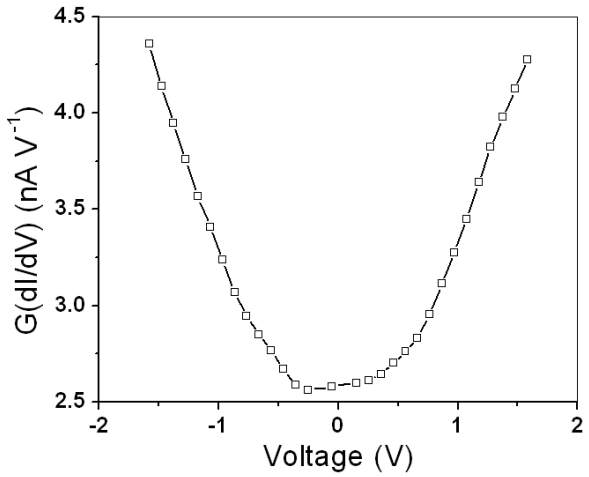

Figure 8. A typical nonlinear conductance curve taken at low temperatures ($T = 20$ K) on the nanowires.

typical current–voltage (I–V) characteristics taken on the sample at different temperatures. The I–V curve shows the onset of nonlinear behavior as the sample is cooled below 100 K and at low temperatures it is strongly nonlinear. The nonlinear conduction, as we show below, changes characteristics at the Peierls transition. The I–V data have been converted into a differential conductivity $G(V) = \mathrm{d}I/\mathrm{d}V$ versus V relation. Typical data are shown in figure 8. It can be seen that there is a substantial reduction in the conductance at the zero bias below the transition temperatures. The $G(V)$ versus V curves can be parameterized by an empirical relation (1):

$$G(V) = G_0 + G_\alpha |V|^n \tag{1}$$

where G_0 is the zero bias conductance, while the coefficient G_α and exponent n measure the nonlinear conduction. We have fitted the I–V curves to (1) and obtained the parameters. Figure 9 shows the variation of the parameters G_0, G_α and n as a function of temperature. G_0 starts to drop as the temperature is lowered below RT and it shows a sharp drop at the transition, which we expect because of the opening of the gap in the charge excitation spectrum at the Peierls transition temperature. There is also a drop in the coefficient G_α. The determination of n becomes somewhat inaccurate due to noise in the data. The value of n is ∼1–1.5 for $T > 50$ K. However, below the transition it increases and the bias dependence becomes stronger. The issues of nonlinear transport are elaborated more in section 4.

4. Discussion

One of the main achievements of the investigation is to establish that this method of fabrication can give molecular wires of charge transfer materials with sufficiently small diameters and of a quality that can sustain phenomena like the Peierls transition. In this investigation we could also go down to low enough temperatures and investigate the temperature dependence of resistance as well as the nonlinear conduction as a function of temperature well below the transition temperatures. It is noted that the observation of the Peierls transition depends on, among other things the coherence in stacking of the TTF and TCNQ stacks. Though there is sufficient disorder in the system (as concluded from the activated transport at higher temperatures), there is enough coherence that the transition can set in.

The resistance does show an activated behavior over the whole temperature range and the transition is seen as a change in the slope as well as the onset of hysteresis behavior. The hysteresis in resistivity appears when the temperature is taken to or below 90 K. It persists even after repeated thermal cycling

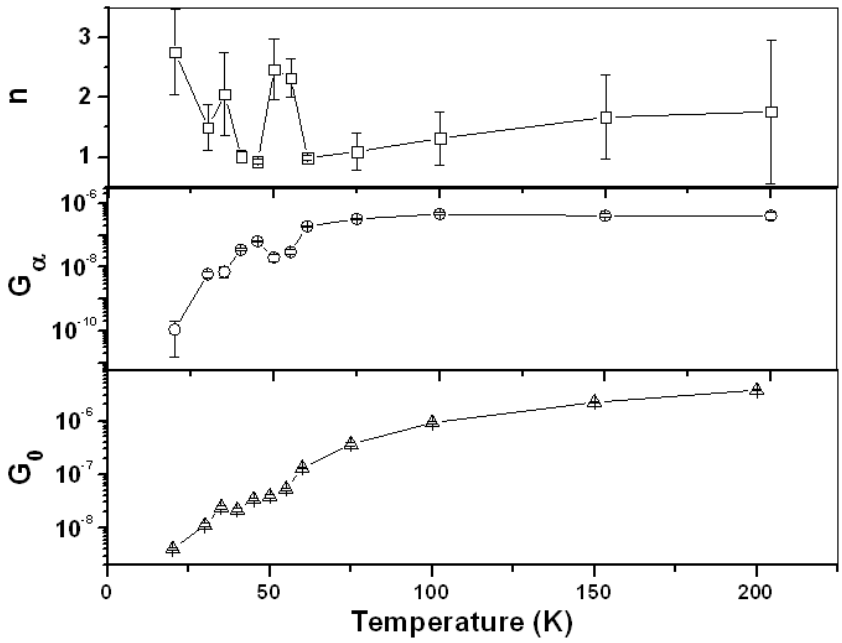

Figure 9. The temperature dependence of the parameters obtained from the fit of the data to (1).

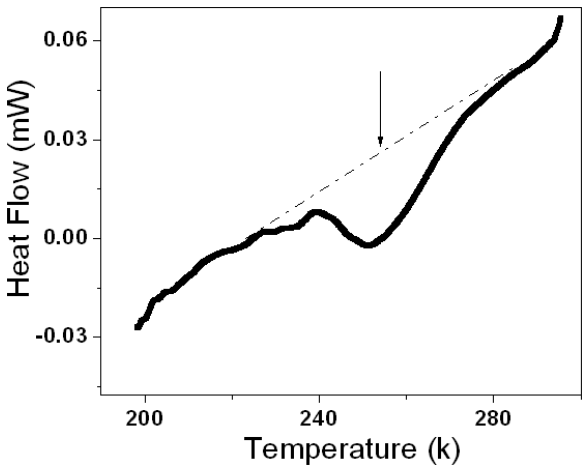

Figure 10. DSC heating curve showing a broad peak around 250 K.

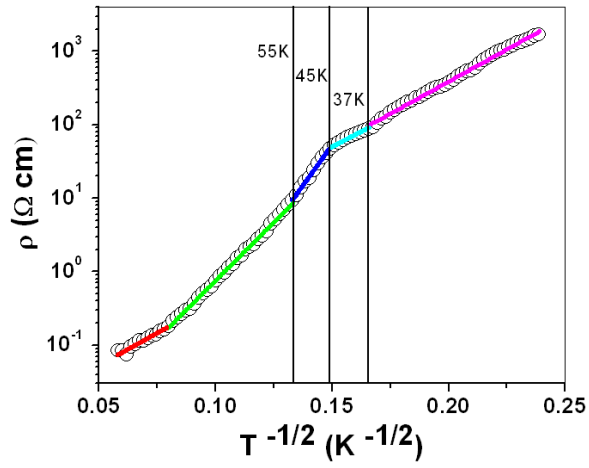

Figure 11. Plot of $\ln \rho$ versus $T^{-1/2}$. The change in slope can be noted at the marked transition temperatures.

although the separation between the heating and cooling curves reduces somewhat after repeated thermal cycling. This type of hysteresis is a new observation and has not been seen in bulk single crystal. (A small hysteresis in resistivity has been reported before by [16] where they saw a small kink in the heating curve at 260 K. However, it has not been investigated.) To check whether there is any thermodynamic signature to the hysteresis seen in resistivity we did a thermal analysis (differential scanning calorimetry (DSC)) of the nanowires grown by evaporation. We find that, while during cooling there is no thermal anomaly, during heating a small and broad endothermic peak occurs around 250 K which is shown in figure 10. The anomaly persists till 265 K. The heating and cooling curves for the resistivity merge with each other after this thermal anomaly is over. Although a detailed discussion on this feature is beyond the scope of the present report, we suggest the following likely cause for this. The difference between the heating and cooling curves shows that the heating curve always has a higher resistivity than the cooling curve. The likely cause of the activated behavior and the higher resistivity in the nanowires in this temperature region is the disorder in the stacking sequence of TTF and TCNQ, as stated before. It may be that during cooling this disorder builds up. When the sample is cooled below 90 K (when the hysteresis appears on cooling), the disorder is frozen in due to a finite activation barrier. On heating beyond 250 K, the frozen disorder can relax through the activation barrier, leading to a merger of the two resistivity curves at higher temperatures. The small endothermic peak seen in the thermal analysis curve is a manifestation of the thermal relaxation of the frozen disorder.

The temperature dependence of resistance was found to obey an activated behavior. The plot of $\ln \rho$ versus $T^{-1/2}$ is shown in figure 11 where a clear change in slopes has been observed between 55 and 37 K, the region where the Peierls transition occurs. The temperature-dependent resistivity cannot be fitted to either Mott or Efros–Shkolvskii type variable range hopping. (For d dimensions the hopping conductivity should follow the relation $\sigma = \sigma_0 \exp(-T_0/T)^{1/1+d}$. Thus in one dimension one would expect resistivity $\rho \propto \exp(T_0/T)^{1/2}$, which is the same as is expected for Efros–Shkolvskii-type hopping.) The transport in this region is highly nonlinear and thus a simple resistance (measured at a fixed current or voltage) may not be the best way to express the transport data. An alternative model to describe the transport can be the trap-assisted transport model [21]. This model in principle can fit the nonlinear conductance data because the current density is related to the electric field by (2)

$$j(E) = \frac{2q}{\tau}\frac{1}{z^2} e^{\frac{-\phi_t}{kT}} \sinh\left(\frac{qzE}{2kT}\right) \qquad (2)$$

where τ is the escape time for the trapped electron, q is the charge, z is the intertrap distance and ϕ_t is the trap depth from the conduction band edge. The data was fitted with τ taken to be 4×10^{-13} s. The data above 50 K can be fitted to the model with an average trap distance of ≈2–2.5 nm. However, the trap depth obtained from the fit becomes strongly temperature-dependent. Thus the model may also be an acceptable model to describe the data above 50 K.

The room temperature conductivity of this sample is 10–12 S cm^{-1}. The fact that the observed conductivity of the nanowires is less than that observed for single crystals (≈500 S cm^{-1}) and thin films (≈30 S cm^{-1}) of TTF–TCNQ would mean that it has a random contribution from σ_a and σ_b, the conductivities along a and b axes, respectively. In single crystals the resistivity shows metallic behavior above the transition. In the nanowires, however, we find activated transport even above the transition temperature, although with rather low activation energy. This most likely arises from the disorder in the stacking sequences of TTF and TCNQ.

The analysis of the G–V curves is shown in figure 9. It can be seen that there is a rapid drop in the zero bias conductance G_0 as the transition is approached. At or below the transition G_0 drops by nearly two orders of magnitude. We would like to investigate whether the drop in conductivity seen at the transition can indeed be interpreted as freezing out of normal single-particle charge transport at or below the Peierls transition. If the transition is the Peierls transition then below the transition the conduction will happen through CDW motion. The transport of CDW in

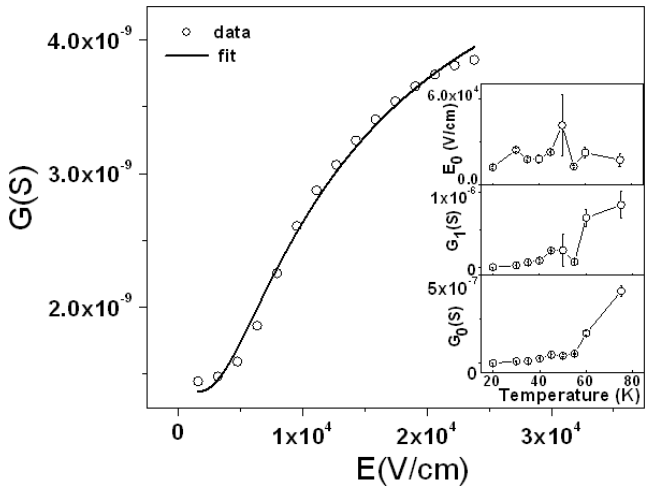

Figure 12. The G–E data at $T = 20$ K shown with best fit obtained for (3). The inset shows the temperature dependence of fitting parameters.

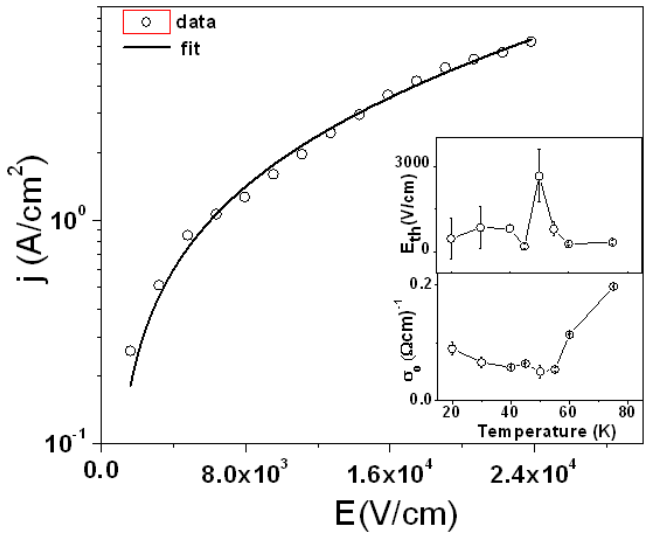

Figure 13. The j–E data at $T = 20$ K shown with best fit obtained for (4). The inset shows the temperature dependence of fitting parameters.

single crystals of a number of conductors showing a CDW transition has been extensively investigated [22, 23]. A number of theories and expressions have been used to describe the CDW transition in bulk single crystals. We refer to published review articles. The predominant theories based on [23] are (a) Zener tunneling [24], (b) the Bardeen model which is a tunneling theory of CDW de-pinning [25] where one associates a threshold field with the phenomena, (c) the FLR model where conductivity of sliding CDW is modeled in the asymptotic limit at applied field E [26] and (d) a creep-like conduction in high field [27]. These relations have been used extensively in the past to investigate the CDW transport in single crystals of inorganic systems like $NbSe_3$. For the molecular wires studied by us, with the length of the wires being small (≈600 nm), even a small applied bias leads to a high field. The transport in these wires thus occurs predominantly in the region $E \geqslant E_T$ for most of the applied bias. We have tried to fit the data to all the models available. While one may have reasonable fits to all the models we find that over an extensive temperature range the data can be fitted to the Zener model where the current conductance $G(E)$ is given by (3)

$$G(E) = G_0 + G_1 \exp[-E_0/E] \qquad (3)$$

where G_0 and G_1 are constants, and E_0 is an energy scale like a gap. A typical fit to (3) at 20 K is shown in figure 12. The fits to the equation were good up to the transition temperature and to somewhat higher temperatures. In the inset of figure 12, the variation of fitting parameters as a function of temperature is shown. From the fits we find that the parameter E_0 is more or less temperature-independent, barring the region around the transition where it shows a large enhancement by a factor of 2. The parameters G_0 and G_1, that provide the conductance scales, increase sharply at the transition temperature.

In the creep-like conduction model current density j is given by (4)

$$j(E,T) = \sigma_0(E - E_{th}) \exp[-T_0/T] \exp[\alpha E/T] \qquad (4)$$

where σ_0 is a constant related to conductivity, T_0 is related to the single-particle gap and α is a fitting parameter. A typical fit to (4) at 20 K is shown in figure 13. The fits were performed by taking $T_0 = 126$ K, which was estimated from the activation energy obtained from the temperature variation of resistivity curves. In the inset of figure 13, the variation of fitting parameters as a function of temperature are shown. The parameter σ_0 which was obtained from the fits increases sharply at the transition, much like G_0. The threshold field E_{th} also shows an interesting dependence. It is more or less temperature-independent below 40 K but shows a large jump at the transition region before becoming zero above the transition. The value obtained for E_{th} shows that the transport predominantly occurs in the region $E \geqslant E_T$. Given the fact that we make measurements on rather short filaments, even moderate voltages give rise to large fields. In single crystals of TTF–TCNQ the observed threshold field was ≈0.25 V cm^{-1} below 54 K, which increases up to 10 V cm^{-1} below 35 K [28]. In general, the presence of impurities and defects enhances the threshold field. The larger threshold field observed by us is thus understandable.

Form the discussion above it appears that the anomaly seen in the electrical transport at around the 37–55 K region can be linked to a Peierls transition and associated phenomena of transport by CDW. De-pinning of the CDW then can be the origin of the nonlinear transport in these nanowires. Study of CDW transport has not been done in such small samples of this dimension before. The availability of these nanosize samples, that show a Peierls transition, thus gives us an opportunity to study the physics of pinning/de-pinning of CDW in a size regime that has not been done before. However, a more quantitative study of the transport will be required, preferably with four-probe measurements on these nanowires to answer the relevant questions. Such a study is beyond the scope of this present report.

5. Conclusions

The molecular wires of TTF–TCNQ have been grown on an SiO_2 substrate by evaporating TTF–TCNQ in the presence of electric field across prefabricated electrodes with gaps in the sub-micron range (∼600 nm). The wires so grown are crystalline and have diameters in the range of 130 nm and are the smallest diameters reported to date. The molecular wires show a charge transfer ratio ∼0.57, close to that seen in bulk crystals. The wires show Peierls transitions at low temperatures. The transition temperatures as determined from the temperature dependence of resistivity are the same as what one sees in bulk single crystals. Below the transition the transport is strongly nonlinear and can be interpreted as originating from de-pinning of CDW, which forms at the Peierls transitions.

References

[1] Coleman L B, Cohen M J, Sandman D J, Yamagishi F G, Garito A F and Heeger A J 1973 *Solid State Commun.* **12** 1125

[2] Reinhardt C, Volmann W, Hamann C, Libera L and Trompler S 1980 *Krist. Tech.* **15** 243

[3] Yase K, Ara N and Kawazu A 1994 *Mol. Cryst. Liq. Cryst.* **247** 185

[4] Garelik S, Vidal Gancedo J, Figueras A, Caro J, Veciana J, Rovira C, Ribera E, Canadell E, Seffar A and Fontcuberta J 1996 *Synth. Met.* **76** 309

[5] Caro J, Garelik S and Figueras A 1996 *Chem. Vapor Depos.* **2** 251

[6] Figuera A, Caro J, Fraxeda J and Laukhinb V 1999 *Synth. Met.* **102** 1611

[7] Fraxedas J, Molas S, Figueras A, Jimenez I, Gago R, Auban-Senzier P and Goffman M 2002 *J. Solid State Chem.* **168** 384

[8] Kistenmacher T J, Philips T E and Lowan D O 1974 *Acta Crystallogr.* B **30** 763

[9] Takahashia Y, Hasegawa T, Abe Y, Tokura Y, Nishimura K and Saito G 2005 *Appl. Phys. Lett.* **86** 063504

[10] Shibata K, Wada H, Ishikawa K, Takezoe H and Mori T 2007 *Appl. Phys. Lett.* **90** 193509

[11] Sakai M, Nakamura M and Kudo K 2007 *Appl. Phys. Lett.* **90** 062101

[12] Chappell J S, Bloch A N, Bryden W A, Maxfield M, Poelher T O and Cowan D O 1981 *J. Am. Chem. Soc.* **103** 2442

[13] Akutagawa T, Ohta T, Hasegawa T, Nakamura T, Christensen C A and Becher J 2002 *Proc. Natl Acad. Sci.* **99** 5028

[14] Liu H, Li J, Lao C, Huang C, Li Y, Wang Z L and Zhu D 2007 *Nanotechnology* **18** 495704

[15] de Caro D *et al* 2000 *C. R. Acad. Sci., Paris* IIc **3** 675

[16] Sakai M, Iizuka M, Nakamura M and Kudo K 2003 *Japan. J. Appl. Phys.* **42** 2488

[17] Sakai M, Iizuka M, Nakamura M and Kudo K 2005 *Synth. Met.* **153** 293

[18] Phanindra Sai T and Raychaudhuri A K 2008 *Mater. Res. Soc. Symp. Proc.* **1058** JJ05-03

[19] Rojas C, Caro J, Grioni M and Fraxedas J *Phys. Rev. Lett.* **40** 1048

[20] Friend R H, Miljak M and Jerome D 1978 *Rev. Mod. Phys.* **60** 1129

[21] Manger D *et al* 2009 *Microelectron. Eng.* **86** 1815

[22] Gruner G 1988 *Rev. Mod. Phys.* **60** 1129

[23] Throne R E 2005 *J. Physique* IV **131** 89

[24] Monceau P, Ong N P, Portis A M, Meerschaut A and Rouxel J 2005 *Phys. Rev. Lett.* **37** 602

[25] Bardeen J 1980 *Phys. Rev. Lett.* **45** 1978

[26] Sneddon L, Cross M C and Fisher D S 1982 *Phys. Rev. Lett.* **49** 292

[27] Lemay S G, Throne R E, Li Y and Brock J D 1999 *Phys. Rev. Lett.* **83** 2793

[28] Forro L, Lacoe R, Bouffard S and Jerome D 1999 *Phys. Rev.* B **35** 5884